ADVANCED MATERIALS
www.advmat.de

Liquid Gating Meniscus-Shaped Deformable Magnetoelastic Membranes with Self-Driven Regulation of Gas/Liquid Release

*Jing Liu, Xue Xu, Yi Lei, Mengchuang Zhang, Zhizhi Sheng, Huimeng Wang, Min Cao, Jian Zhang, and Xu Hou**

Liquid gating membranes have been demonstrated to show unprecedented properties of dynamicity, stability, adaptivity, and stimulus-responsiveness. Most recently, smart liquid gating membranes have attracted increasing attention to bring some brand-new properties for real-world applications, and various environment-driven systems have been created. Here, a self-driven system of a smart liquid gating membrane is further developed by designing a new sytem based on a liquid gating magnetoelastic porous membrane with reversible meniscus-shaped deformations, and it is not subject to the complex gating liquid restriction of magnetorheological fluids. Compared with other systems, this magnetic-responsive self-driven system has the advantage that it provides a universal and convenient way to realize active regulation of gas/liquid release. Experiments and theoretical calculations demonstrate the stability, the nonfouling behavior, and the tunability of the system. In addition, this system can be used to perfectly open and close gas transport, and the gating pressure threshold for the liquid release can be reduced under the same conditions. Based on the above capabilities, combined with the fast and 3D contactless operation, it will be of benefit in fields ranging from visible gas/liquid mixture content monitoring and energy-saving multiphase separation, remote fluid release, and beyond.

1. Introduction

As rationally designed liquid-based adaptive materials, liquid gating membranes have exhibited great performance of nonfouling and energy efficiency over traditional membranes, benefiting from their reconfigurable and reversible opening and closing liquid gate.[1] With capillary-stabilized liquid sealing the pores distributed randomly or uniformly, both gases and liquids can be transported and released in a controlled manner through liquid gate drawing on the partnership of static solid porous membranes with dynamic adaptive liquids.[2] The dynamic interfacial interaction between these two phases contributes to the development and design of sophisticated and versatile liquid gating membrane systems, enabling them to create new opportunities for smart materials and find ways into increasing energy, biomedical, and environmental and resource management scenarios, such as multiphase separation,[3] drug delivery,[4] chemical detection,[5] and chemical reaction.[6]

In pursuit of further advancing diversified functions and bringing widespread applications, the common strategy is to develop smart liquid gating membranes in response to a single or multiple synergistic external stimuli,[1a,7] such as light, temperature, electric fields, magnetic fields, pH, and specific ions/molecules.[8] General approaches for the responsive interface design of smart liquid gating membranes have focused on responsive gating liquid design and responsive solid porous membrane design.[2c,9] Recent works have achieved some steps toward this approach. For example, relying on the 1D or 2D stretching deformation of an elastomeric material in response to a mechanical stimulus, a liquid gating elastomeric porous membrane system has

J. Liu, X. Xu, Z. Sheng, H. Wang, M. Cao, J. Zhang, X. Hou
State Key Laboratory of Physical Chemistry of Solid Surfaces and Department of Chemistry
College of Chemistry and Chemical Engineering
Xiamen University
Xiamen 361005, China
E-mail: houx@xmu.edu.cn

The ORCID identification number(s) for the author(s) of this article can be found under https://doi.org/10.1002/adma.202107327.

DOI: 10.1002/adma.202107327

Y. Lei, M. Zhang, X. Hou
Department of Physics
Research Institute for Biomimetics and Soft Matter
Fujian Provincial Key Laboratory for Soft Functional Materials Research
Jiujiang Research Institute
College of Physical Science and Technology
Xiamen University
Xiamen 361005, China

Z. Sheng
Suzhou Institute of Nano-Tech and Nano Bionics
Chinese Academy of Sciences
Suzhou 215123, China

X. Hou
Tan Kah Kee Innovation Laboratory
Xiamen, Fujian 361102, China

been developed for dynamic controllable gas/liquid transport under steady-state environmental pressure.[3b,10] In addition, by confining the magnetic colloids of a magnetorheological fluid (MRF, as the gating liquid) in a rigid copper foam, the mechanical properties of the colloidal particles can be modulated through the magnetic field, which opens up new avenues for functional gating liquid design. The presence of the magnetic field acted as a resistance to increase the gating threshold pressure to realize passive regulation of gas/liquid release.[4a] More recently, based on the light-responsive solid porous substrate or photothermal induced liquid gate, smart liquid gating systems that use light to navigate fluid transport have been developed.[6,11] Although much progress has been made in various stimulus-response systems that rely on the environmental pressure to drive them, a self-driven liquid gating system has not yet been realized, which is very important in many practical applications without environment-driven conditions.

In this work, we present a self-driven system based on a liquid gating magnetoelastic porous membrane (LGMPM), and demonstrate active gas/liquid release regulated by magnetic-responsive meniscus-shaped deformations. When the external magnetic field was applied, the magnetoelastic membrane (MM) deforms into a meniscus shape in 3D space, and the deflection can be precisely controlled under different magnetic field strengths theoretically and experimentally. On the basis of rational interfacial design, the deformation of magnetoelastic porous membrane (MPM) expands the aperture of pores to reduce the gating pressure threshold of the transport fluid, and allows for remote gas and liquid release in an active regulatory mode. Moreover, by converting the magnetic force into mechanical force directly acting on the fluid, environmental-pressure-driven equipment is not necessary, which makes this magnetic-responsive system fully self-driven for releasing and controlling the release amount under different external magnetic fields. Enabling self-driven release regulation for smart liquid gating membranes is an important step toward realizing smart visual monitoring, on-demand drug delivery in local disease treatment, and miniaturized and portable integration for various engineering processes.

2. Results and Discussion

2.1. Preparation and Self-Driven Mechanism of the Liquid Gating Magnetoelastic Porous Membranes

The fabrication procedure and self-driven gas/liquid release mechanism of the liquid gating magnetoelastic porous membrane are shown schematically in **Figure 1**. Magnetoelastic materials exhibit a variety of advantages including remote and quick response, high actuation strain, as well as high controllability.[12] The mechanical properties of the MRF can undergo significant changes and be magnetized/demagnetized at the millisecond timescale under the influences of a magnetic field.[13] When continuous-phase MRF was incorporated into the elastomer, more effective changes in mechanical properties will

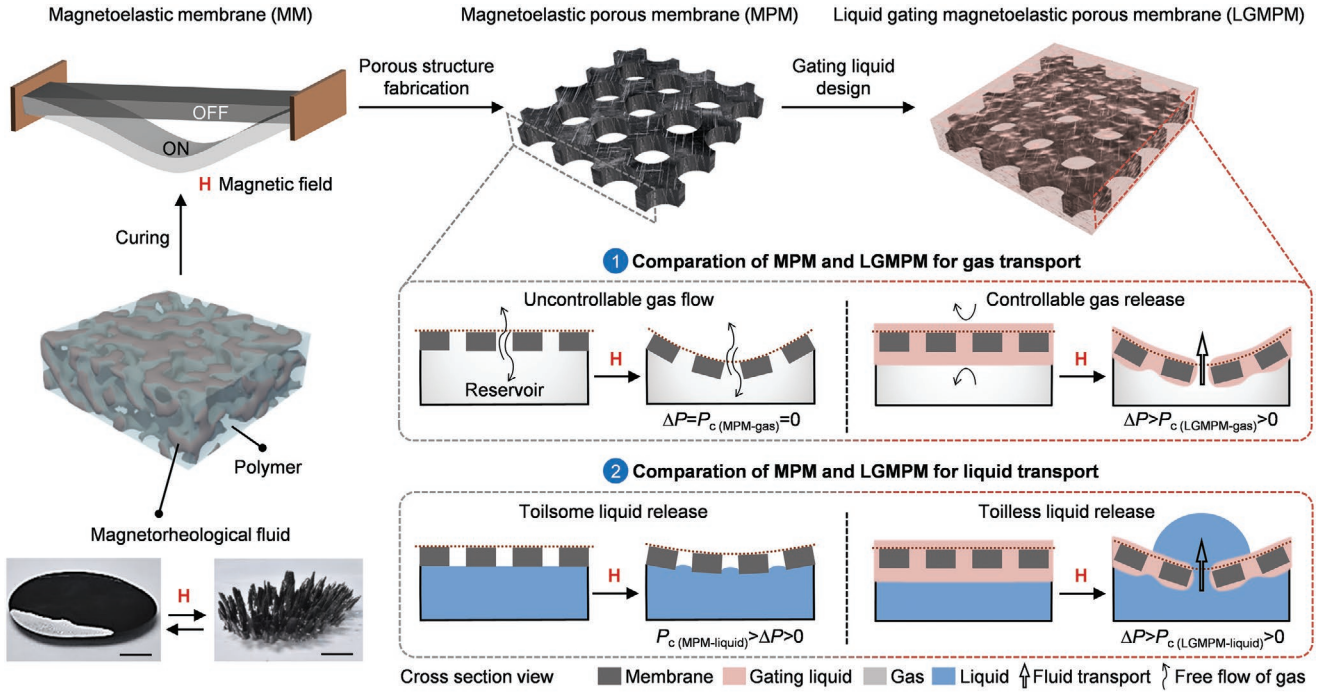

Figure 1. Preparation of the liquid gating magnetoelastic porous membrane (LGMPM) and schematics of self-driven gas/liquid release. Magnetoelastic membrane (MM) composes of magnetorheological fluid (MRF) and polymer elastomer matrix. The response behavior of the MRF to the external magnetic field leads to the meniscus-shaped spatial deformation of the MM. The magnetoelastic porous membrane (MPM) is fabricated from the MM by laser cutting, and after infiltrating the gating liquid, the LGMPM is formed. Gas can flow freely through the MPM without being controlled, while the LGMPM can actively control gas release driven by the magnetic field. Under the same magnetic field condition, compared to the MPM, it is easier for the liquid to be released through the LGMPM with a lower critical transmembrane pressure. Scale bars: 5 mm.

be realized.[12d,14] Therefore, by encasing commercial MRF droplets in a poly(dimethylsiloxane) (PDMS) elastomer matrix and after curing, we manufactured an MM with exceptional magneto-mechanical properties (Figure S1, Supporting Information). An MRF was used here to build the magnetic actuation. Under an applied magnetic field, 3D deformation of this soft elastic composite can be easily achieved. Through the laser cutting method, an MPM with porous arrays can be obtained from the MM. Then the LGMPM was constructed by infiltrating the MPM with a suitable functional gating liquid.

The MPM and the LGMPM have different control capabilities in fluid transport. For gas transport, regardless of whether a magnetic field is applied or not, gas can flow freely in and out of the porous arrays without being controlled by the MPM. However, for the LGMPM, the capillary-stabilized gating liquid is filled in the pores inducing the competition between the interfacial tension and the applied pressure (ΔP). The gas must break the interface of the filled liquid to be released from the reservoir. The minimum pressure required is called the transmembrane critical pressure (P_c). When no magnetic field is applied, the liquid gate is closed, and the gas can be stably stored in the reservoir without leakage ($P_{c(\text{LGMPM-gas})} > \Delta P = 0$). Once the magnetic field is applied, the LGMPM deforms into a meniscus shape and the liquid gate is opened to achieve self-driven gas release ($\Delta P > P_{c(\text{LGMPM-gas})} > 0$). For liquid transport, under the same magnetic field, the liquid release is difficult for the MPM but can be facilely achieved through the LGMPM, where the gating liquid acts as a lubricating layer to make the critical pressure lower ($P_{c(\text{LGMPM-liquid})} < P_{c(\text{MPM-liquid})}$).[2b]

2.2. Magnetic and Mechanical Properties of Magnetoelastic Membranes

We dispersed MRF droplets with different contents ranging from 10 to 25 wt% in PDMS before cross-linking. The morphology of the MM was observed by scanning electron microscope (SEM) shown in Figure S1 (Supporting Information). The results show that the magnetic particles were homogeneously distributed in the PDMS matrix with a small fraction of aggregation. With the increase in MRF content, both the number and size of magnetic particle agglomerations may increase, and the distribution of the magnetic particles in the cured MM would not change under the applied magnetic field (Figure S2, Supporting Information). In order to understand the effect of the MRF content dispersed in the polymer matrix on the magnetic properties of the composites, we tested the hysteresis loops at room temperature for the MM samples (**Figure 2**a). The same hysteretic and reversal behavior was shown in the magnetization curves, and both the remanence magnetization and the coercivity of the composites are very low, almost negligible, making them easy to be demagnetized.[12f,15] As expected, the saturation magnetization of composites increases with increasing the MRF content. This result suggests a uniform distribution and occasional aggregation of magnetic particles in the matrix, which confirms the analysis of the SEM images. Although the sample with an MRF content of 25 wt% has the largest saturation magnetization, the curing time becomes longer due to the incorporation of more carrier fluid in the MRF containing a mixture of simethicone, mineral oil, and other additives.[13a] Considering the production cost and the curing time, we chose MRF/PDMS composites with a content of 20 wt% MRF as the substrate for establishing the LGMPM in the following measurements unless stated otherwise.

We further investigated the mechanical properties of the pure PDMS and the MM with 20 wt% by measuring the stress–strain curves in the absence of a magnetic field (Figure 2b). Pure PDMS exhibits a higher tensile strength of 6.5 MPa but a lower maximum strain of 213%. With the incorporation of MRF, due to the immiscibility between the carrier fluid of MRF and PDMS (Figure S3, Supporting Information), the oil droplets reduced the cross-linking density in PDMS, resulting in the tensile strength of the MM being decreased to 2.3 MPa. However, the maximum strain was significantly increased up to 404% with the Young's modulus of 0.38 MPa for the MM, indicating that the stretchability can be improved by incorporating a small amount of MRF. Generally, the main reason for the increase of strain at break is attributed to specific interactions between the polymer matrix and fillers, such as strong H-bonds that play the most important role in the high stretchability of MM.

The MM has an excellent mechanical response to the external magnetic field generated by a permanent magnet (Figure S4, Supporting Information). With the magnetic field on, due to the effect of the magnetic field gradient, the magnetic force perpendicular to the surface actuates the MM to bend toward the magnet. The bending deformation behavior of the MM is exclusively caused by accumulating the magnetic interaction among magnetic particles and the strong bonding between the particles and the elastomer matrix.[16] The corresponding initial state on the top side indicates the softness and good flexibility of the MM. To further evaluate the magnetic-responsive property of the composite membranes, we also conducted the deflection measurements and theoretical stimulation by COMSOL Multiphysics on the MM under different magnetic field strengths (Figure 2c,d). The displacement of the MM is driven and controlled by the magnetic field, and the final shape is determined by the balanced interaction of magnetic forces and elastic resistance.[17] The magnetic field is provided by three bar permanent magnets with countersunk holes, and the MM was aligned in the middle of them. We measured the magnetic field distribution with a Gauss meter and meanwhile performed numerical simulations (Figures S4 and S5, Supporting Information). Under the applied magnetic field, the MM has the largest deformation height in the center and gradually decreases to the surroundings, indicating that the deformation is a meniscus shape in the 3D space. As the magnetic field strength increases, the deflection of the sample increases significantly. In the experiment, under an external magnetic field of 220 mT, the maximal deflection is 224 µm. Similarly, the elastic strain energy density at the center of the sample is also the largest with the impact of magnetoelastic interaction. Therefore, we designed the porous structure in the center of the membrane to maximize the use of energy and deformation.

2.3. Stable Liquid Gating Magnetoelastic Porous Membranes

Figure 2e shows the optical microscopy images of an MPM made from the MM by laser cutting methods, demonstrating

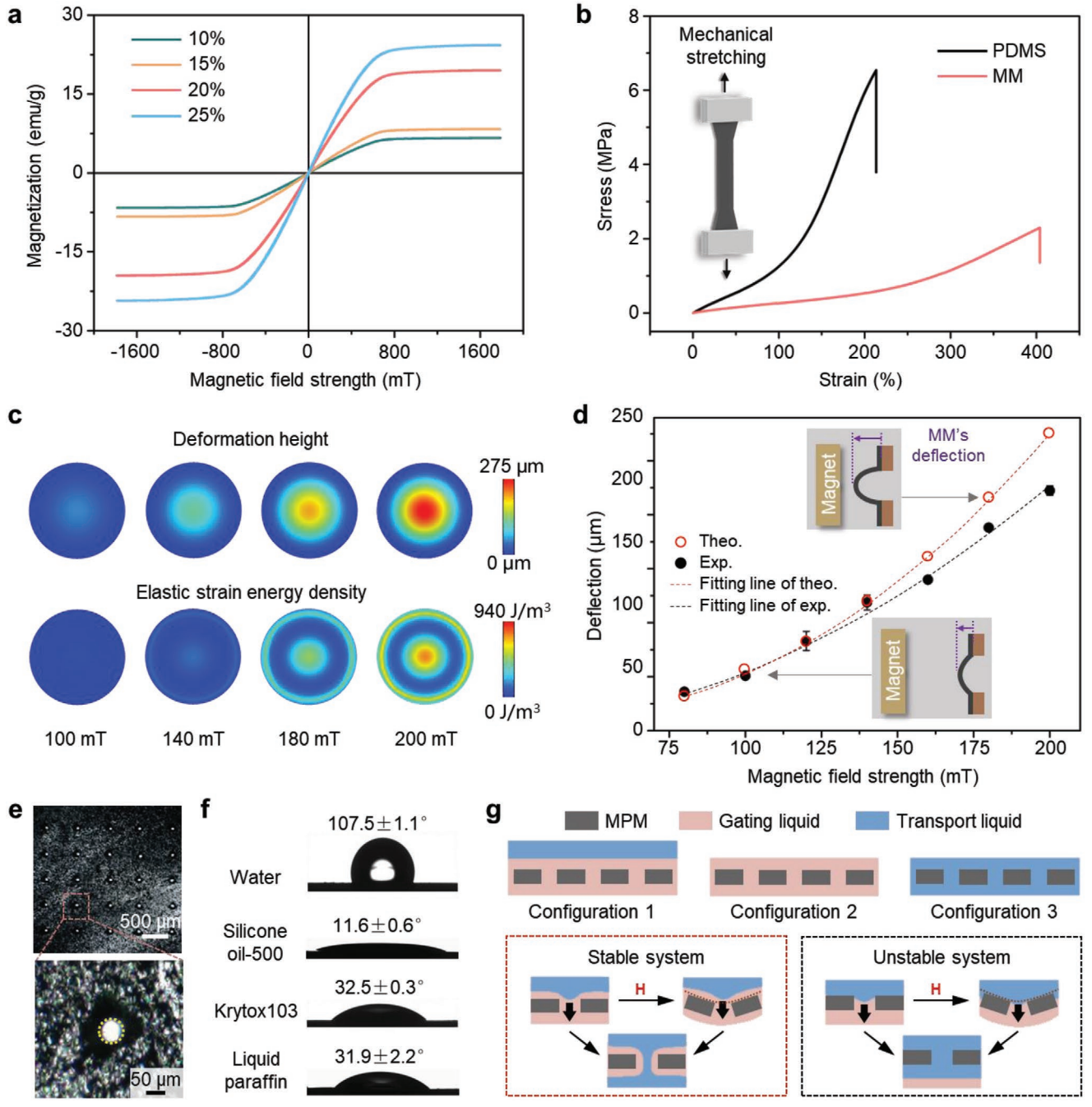

Figure 2. Properties of the magnetoelastic membranes (MMs). a) Magnetization versus magnetic field strength for the magnetoelastic membrane with different magnetorheological fluid (MRF) contents. b) Stress–strain behavior of pure poly(dimethylsiloxane) (PDMS) membrane and an MM with 20 wt% MRF. c) A series of simulations of deformation height maps at increasing magnetic field strengths, together with the elastic strain energy density maps, show that the thin sheet of MM morphs into the 3D meniscus shape. d) Deflections at different applied magnetic fields for the MM. Inset diagrams: the MM's deflections under different magnetic fields strength. e) Optical microscopy images of magnetoelastic porous membrane (MPM) with porous array structure are fabricated by laser cutting. f) The wettability of the MM. The CA of water, silicone oil-500, Krytox 103, and liquid paraffin were tested on a solid magnetic elastomeric membrane without the magnetic field. g) Schematics of different configurations, as well as the transport processes of stable and unstable liquid gating magnetoelastic porous membrane (LGMPM) systems.

a homogeneous porous array distribution with an average pore size of ≈50 μm (Figure S6, Supporting Information). The aperture can be effectively controlled by adjusting parameters such as laser power and cutting speed. Another whole membrane with 25 uniform pores (pore size of ≈120 μm) in the center is shown in Figure S7 (Supporting Information). We designed the stable liquid gating system, which requires a strong affinity between the gating liquid and the solid membrane material, and the gating liquid will not be displaced by the transport liquid. By measuring the wettability of the transport liquid and

different gating liquids on the MM substrates, the contact angle (CA) of water, silicone oil-500, Krytox 103 oil, and liquid paraffin were shown in Figure 2f. Water shows a CA of 107.5 ± 1.1°. Krytox 103 and liquid paraffin have CA values of 32.5 ± 0.3° and 31.9 ± 2.2°, respectively. Silicone oil-500 has the lowest CA of 11.6 ± 0.6° with the best affinity on the MM to enable complete wetting. Moreover, there is almost no difference in testing CA under an applied magnetic field of 220 mT (Figure S8a, Supporting Information), indicating that the magnetic field will not affect the wettability of the MM and the gating liquid. We also conducted the infrared thermal images on the MM, and the results show that there was no thermal effect under the magnetic field applied (Figure S8b, Supporting Information), indicating the suitability of the MM in a constant temperature environment, and the feasibility in biomedicine and other temperature-sensitive applications. To satisfy the requirement of the transport liquid not displacing the gating liquid, we compared the total interfacial energies of the following three configurations (Figure 2g): the solid porous membrane is infiltrated by a gating liquid with (configuration 1, E_1) or without a transport liquid floating on it (configuration 2, E_2), and the solid porous membrane is infiltrated by the transport liquid (configuration 3, E_3). In order to verify the solid membrane has a preferential affinity with the gating liquid, the conditions $\Delta E_{\mathrm{I}} = E_3 - E_1 > 0$ and $\Delta E_{\mathrm{II}} = E_3 - E_2 > 0$ should be satisfied.[3b,18] ΔE_{I} and ΔE_{II} are interpreted as

$$\Delta E_{\mathrm{I}} = \mathrm{R}(\gamma_{\mathrm{B}}\cos\theta_{\mathrm{B}} - \gamma_{\mathrm{A}}\cos\theta_{\mathrm{A}}) - \gamma_{AB} \quad (1)$$

$$\Delta E_{\mathrm{II}} = \mathrm{R}(\gamma_{\mathrm{B}}\cos\theta_{\mathrm{B}} - \gamma_{\mathrm{A}}\cos\theta_{\mathrm{A}}) + \gamma_{\mathrm{A}} - \gamma_{\mathrm{B}} \quad (2)$$

where R is the roughness factor of the MPM ($R = 2$), which is the ratio between the actual and projected surface areas. γ_{A} and γ_{B} are the surface tension of the transport liquid and the gating liquid, γ_{AB} is the interfacial tension between them. θ_{A} and θ_{B} are the equilibrium CAs of the transport liquid and the gating liquid on a flat MM surface, respectively.

Theoretically, if ΔE_{I} and ΔE_{II} are both positive values, the LGMPM is a stable system, if both are negative, the LGMPM tends to be unstable. Based on the energy relationship in **Table 1**, different LGMPMs with various gating liquid/transport liquid combinations were analyzed. We found that using silicone oil-500, liquid paraffin, and Krytox 103 as the gating liquid to transport deionized (DI) water can ensure that the LGMPM system is stable both theoretically and experimentally. Additionally, since silicone oil-500 has the best affinity with the MM, as shown in the previous CA test results, it was selected as the gating liquid to build a stable LGMPM system for the following research.

2.4. Fluid-Transport Behavior of Liquid Gating Magnetoelastic Porous Membranes

To characterize the transmembrane behavior of fluids in the LGMPM system, the critical pressures of the gas and liquid required to pass through the MPM and LGMPM were measured with the magnetic field on and off, respectively. The fluid is transported under a flow rate of 0.5 mL min^{-1}. There are substantial differences between the transmembrane critical pressures of the gas and liquid when flowing through the MPM and LGMPM (**Figure 3**a). For the MPM, regardless of whether there is a magnetic field, the critical pressure of the gas is zero, so that the gas transportation cannot be controlled as mentioned above. Notably, in contrast to the MPM, the LGMPM displays the critical pressure of the gas as 730 ± 8 Pa when the magnetic field is turned off and decreases to 614 ± 15 Pa when the magnetic field is turned on. Therefore, the gas can be released through the LGMPM in a controllable manner by the response of the magnetic field. Besides, the P_{c} required for the LGMPM to transport liquids is lower than that of the MPM. When the external magnetic field was applied, the composites with elastic deformation expand the apertures of the pores. Based on this response model, for the same transport system, a significant decrease in critical pressure was observed $P_{\mathrm{c(on)}} < P_{\mathrm{c(off)}}$, where $P_{\mathrm{c(on)}}$ and $P_{\mathrm{c(off)}}$ are the critical pressure under the condition of the magnet on and off, respectively. After alternately cyclic transport of gas and liquid flowing through the LGMPM, we further demonstrate the stability of this interfacial configuration experimentally (Figure 3b).

Due to the difference of critical pressure between gas and liquid transport ($P_{\mathrm{c(LGMPM\text{-}gas)}} < P_{\mathrm{c(LGMPM\text{-}liquid)}}$), the LGMPM can be employed for separating the gas/liquid mixture in the presence and absence of the magnetic field (Figure 3c and Figure S9a, Supporting Information). Here, the gas is air, and the liquid is DI water dyed red. They are mixed at a flow rate of 1:1 to form a gas/liquid mixed stream. The gas with the lower critical pressure penetrates the membranes to the relief port

Table 1. Comparison of theoretical relationship with experimental results for various gating liquid/transport liquid combinations.

Case no.	Transport liquid (A)	Gating liquid (B)	γ_{A} [mN m^{-1}]	γ_{B} [mN m^{-1}]	γ_{AB} [mN m^{-1}]	θ_{A} [°]	θ_{B} [°]	ΔE_{I} [mN m^{-1}]	ΔE_{II} [mN m^{-1}]	Stable system	
										Theo.	Exp.
1	Deionized (DI) water	Silicone oil-500	72.4	17.4	35.8	107.5	11.6	41.8	132.6	Y	Y
2	DI water	Liquid paraffin	72.4	29.6	41.6	107.5	31.9	52.2	132.6	Y	Y
3	DI water	Krytox 103	72.4	17.7	53.7	107.5	32.5	19.7	128.1	Y	Y
4	Liquid paraffin	Silicone oil-500	29.6	17.4	0.4	31.9	11.6	−16.6	−4.0	N	N
5	Liquid paraffin	Krytox 103	29.6	17.7	11.0	31.9	32.5	−31.4	−8.5	N	N
6	Silicone oil-500	Krytox 103	17.4	17.7	9.8	11.6	32.5	−14.0	−4.5	N	N

The parameters are measured at room temperature (25 °C).

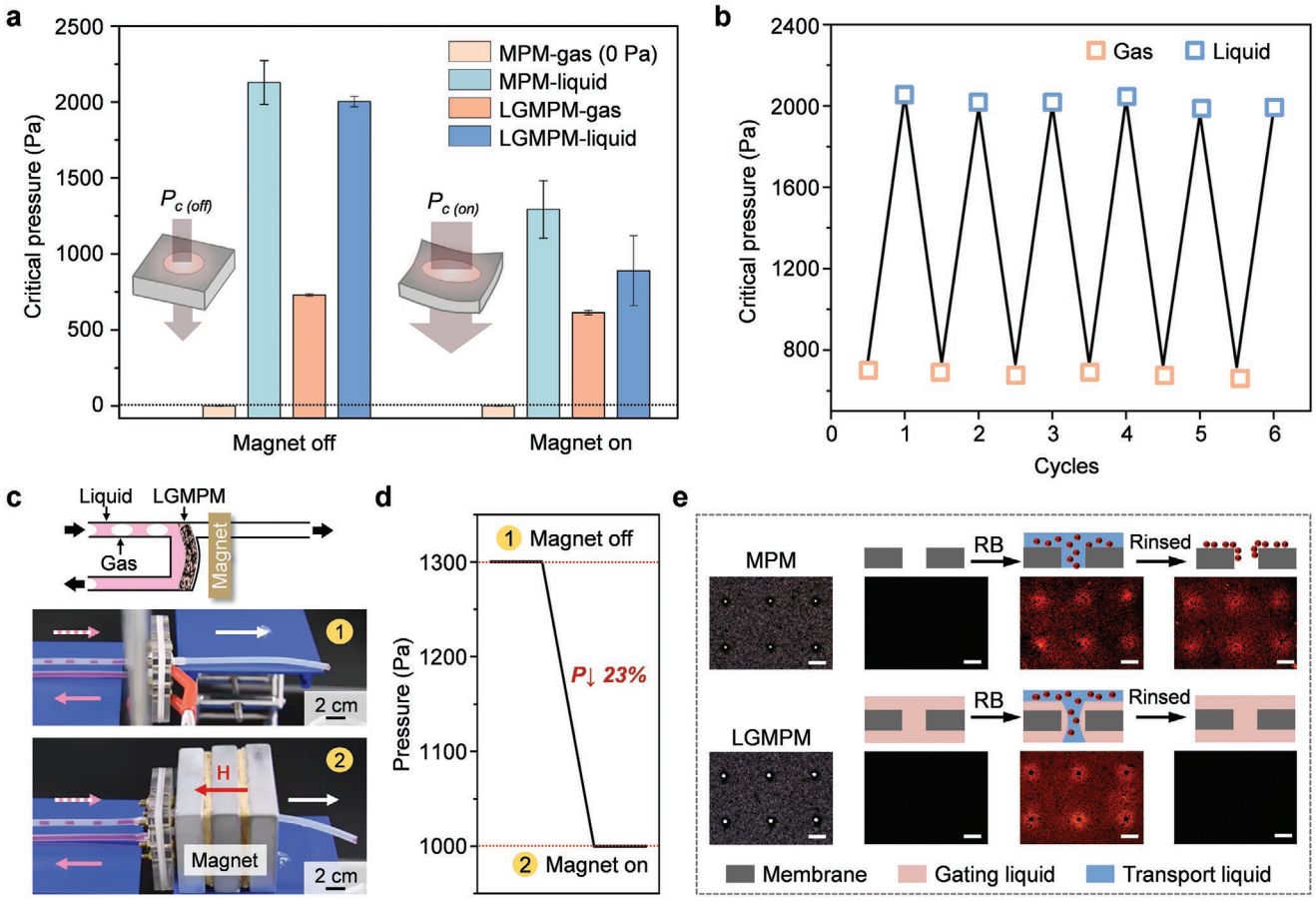

Figure 3. The gating behavior, cyclic stability, gas/liquid separation, and antifouling behavior of liquid gating magnetoelastic porous membranes (LGMPMs). a) Critical pressures of gas and liquid flowing through the magnetoelastic porous membrane (MPM) and LGMPM without and with the magnetic field (H = 220 mT). Here, the gas is air, and the liquid is deionized (DI) water. The insets show the brief schemes of the pore's aperture changes with the magnetic field on and off. b) Cyclic test of alternate transport of gas and liquid through the LGMPM. c) The snapshots of gas/liquid separation processes through the LGMPM (the average pore size of 70 µm, 5 × 5 array) in the presence and absence of a magnet. Top: schematic of experiment in the presence of a magnet. d) The pressure required to separate gas/liquid mixture through the LGMPM in the presence of magnet is 23% lower than in the absence of magnet. e) Antifouling behavior of the LGMPM (bottom) in comparison to the MPM (top). Both the MPM and the LGMPM are treated with rhodamine B (RB) solution and then rinsed with DI water. Scale bars: 200 µm.

while the liquid with the higher critical pressure is blocked and flows to the outlet. Furthermore, since the magnetic-field-driven membrane deformation induces a pressure decrease, the gas/liquid separation process under the magnetic field saves 23% energy compared to the case of no magnet (Figure 3d). The energy-saving rate (for the same liquid gating system, only applying an external magnetic field to reduce the critical pressure, without changing the design and fabrication of the solid porous membrane and the gating liquid), is scaled as $(P_{c(\text{off-mixture})} - P_{c(\text{on-mixture})})/P_{c(\text{off-mixture})}$, where $P_{c(\text{on-mixture})}$ and $P_{c(\text{off-mixture})}$ are the pressure of the LGMPM during gas/liquid separation with the magnet on and off, respectively.

Moreover, the LGMPM also exhibits excellent antifouling properties as illustrated in Figure 3e, which is very important in the membrane separation processes.[19] Before transporting the rhodamine B (RB) solution, neither the MPM nor the LGMPM showed any fluorescence. However, an obvious trace was left on the membrane surface after RB flowed through. After rinsing with DI water, the MPM still retained the fluorescence signal. Conversely, no fluorescence in the LGMPM indicates its good antifouling properties. It is attributed to the existence of a stable liquid–liquid interface between the gating liquid and the transport liquid to prevent the latter from directly contacting the solid material.

2.5. Applications of Liquid Gating Magnetoelastic Porous Membranes

As the practical applications, we applied our LGMPM to demonstrate remote gas and liquid release control and gas/liquid mixture content monitoring. Controlled gas release plays an important role in the field of chemical reactions,[20] soft actuators and robots,[21] and biomedicine.[22] To make an LGMPM-based gas release device, we resorted to a chromogenic reaction for the convenience of observation by selecting a red droplet of phenolphthalein aqueous solution containing $Ca(OH)_2$ (pH = 10.4) placed above the LGMPM with CO_2 as the demo release gas (**Figure 4**a and Figure S9b, Supporting Information). Under a constantly applied pressure (ΔP), the gas was

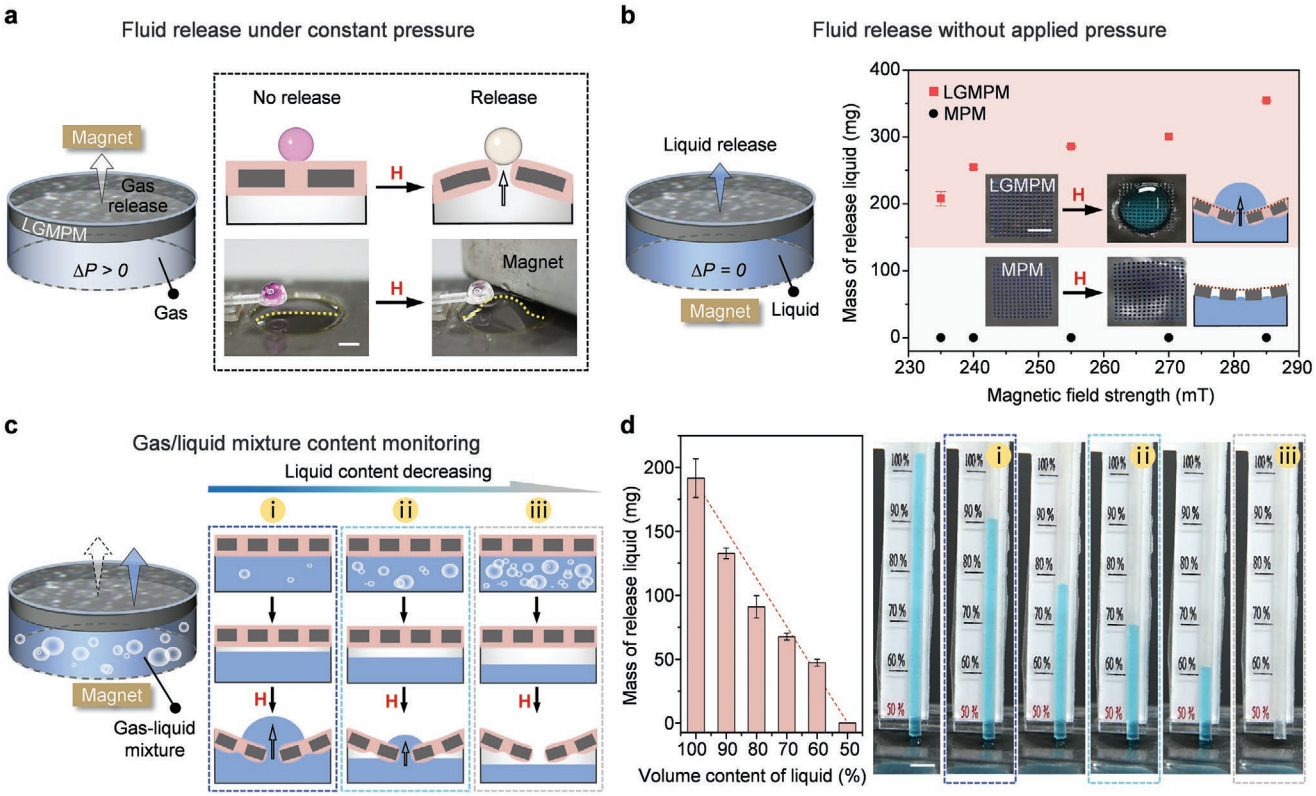

Figure 4. Application demonstrations of liquid gating magnetoelastic porous membranes (LGMPMs). a) Magnetic-field-controlled gas release under a steady-state pressure ($\Delta P = 700$ Pa). Left: Schematic showing the controlled gas release. Right: Snapshots for the comparison of gas release-triggered chromogenic reaction in the case of magnet on and off. The inset schematics demonstrate the difference of reaction in the two cases. b) Magnetic.field. controlled liquid release through self-driven regulation, without additional pressure input ($\Delta P = 0$ Pa). Left: Schematic showing the controlled liquid release. Right: The mass of methylene blue (MB) released by the LGMPM and the magnetoelastic porous membrane (MPM) under different magnetic field stimulation. The photographs show the MB released by the LGMPM and not released by the MPM under the same magnetic field strength of 220 mT. c) Magnetic-field-controlled gas/liquid mixture content monitoring. Left: schematic showing the mechanism of the LGMPM monitoring gas/liquid content by magnetic field stimulation. Right: The top row shows a series of representative schematics of gas/liquid mixture in the reservoir with gradually decreasing liquid content; the middle row shows the gas/liquid mixture layered up and down at the moment of standing; the bottom row shows the corresponding mass of liquid release decreasing with liquid content. d) Left: Relationship between the liquid volume content and the mass of liquid release under the same magnetic field strength. Right: Prototype device for visual liquid content monitoring in gas/liquid mixture. All scale bars: 5 mm.

held without being released, owing to the pores are sealed by capillary-stabilizing gating liquid ($\Delta P < P_{c(off)}$). When the magnetic field is on, as the critical pressure was decreased caused by the membrane deformation ($\Delta P > P_{c(on)}$), CO_2 was released through the opening liquid-lined pores to induce the chromogenic reaction, and the color of the droplet became lighter to colorless. After that, the pores could recover to the closed state to prevent the continuous release when the magnetic field was removed. And we also used a closed chamber with only a small relief port on the top to show more obvious color changes (Figure S9c, Supporting Information).

Moreover, by converting magnetic force into mechanical force, we demonstrated the LGMPM self-driven controlled liquid drug release under magnetic field stimulation (Figure 4b). The reservoir was filled with methylene blue (MB) as a hydrophilic drug model and sealed with the LGMPM (Figure S10, Supporting Information). When the applied magnetic field strength is greater than 220 mT, the membrane deformation induced by the external magnetic field could build up pressure inside the reservoir, which triggers the liquid drug release through the LGMPM. The active regulated on-demand amount of drug delivery may be controlled by adjusting the strength of the external magnetic field, which increases as the strength of the magnetic field increases. However, if we seal the liquid drug with the MPM, there was no liquid released even in the maximum experimental magnetic field. Therefore, in contrast with the MPM, the LGMPM can release liquid drugs more toiless in a smaller magnetic field strength owing to the function of the lubricating layer as described previously, which can be used in a safer and more moderate magnetic environment. Besides, using the mechanical pressure exerted by a magnetic field to regulate fluid transport, a self-driven control method, without the need for any complex additional pressure supply equipment, which has application potential for untethered fluid release in the confined and enclosed spaces.

The remote spatial deformation response of the LGMPM not only has controllable gas and liquid release functions, but also provides a novel method for a wide range of applications as a visible gas/liquid mixture content monitor, especially for the mining, storage, and deep processing of petroleum, chemical,

and natural gas.[23] The LGMPM is acted as a sealing cover to allow the gas/liquid mixture to be stably stored in the reservoir without leakage, and will only be released under the actuation of a magnetic field (Figure 4c). The gas/liquid mixture in the container is immediately layered up and down. At the same magnetic field strength (220 mT), the mass of release liquid across the LGMPM will decrease as the proportion of liquid contained in the reservoir decreases (Figure 4d). While the volume ratio of liquid is less than 50%, no more liquid will be released, which can be used as a warning that the gas content is too high. Therefore, the ratio of the storage gas/liquid mixture can be monitored by the mass of liquid released under a specific magnetic field actuation. We further designed a prototype device, once close to the magnet, the liquid content in the mixture can be directly observed from the height of the liquid released through the LGMPM in the tube (Video S1, Supporting Information). The lower limit of the liquid storage content monitoring is coordinated by the diameter, depth of the reservoir, the strength of the magnetic field, and the pore size of the MPM. This preliminary proof-of-concept demonstrates that the LGMPM could be employed for stably storing the gas/liquid mixture and remotely evaluating and monitoring the gas/liquid content by magnetic field stimulation without external power sources, which will enable the portability for various engineering processes.

3. Conclusion

We have shown a new LGMPM with meniscus-shaped deformation under an applied magnetic field, in which the use of the magnetic field as a mechanical force makes it possible to achieve self-driven regulation of gas/liquid release. The elastic deflection of the MM, the interfacial design and nonfouling behavior of the LGMPM system, and the stability of gas and liquid transport have been discussed theoretically and experimentally. Based on this system, controllable gas-transport opening and closing were realized, and the gating pressure thresholds for liquid transport were reduced. We have also demonstrated representative examples of this noncontact magnetically deformed liquid gating system to showcase the potential application of the LGMPM. Furthermore, since the magnetic fields penetrate various environments, we expect this new self-driven gas/liquid-release mechanism can also provide a universal and green strategy to find uses in future technological areas, including energy exploitation and storage, medical devices, and aerospace.

4. Experimental Section

Fabrication of the Magnetoelastic Membranes: The MMs were prepared by mixing 4 g PDMS (Dow Corning SYLGARD184, with 10% curing agent) and silicone oil-based MRF (MF-112, density 2.5 g cm^{-3}, Henan Huya Trading Co.) in mass fractions of 10, 15, 20, and 25 wt%, as shown in Figure S1 (Supporting Information). The magnetic spherical particles were carbonyl iron particles with a particle size of 2.3 ± 0.2 μm. The mixture was stirred manually for 5 min and placed in a vacuum drying oven for 30 min (DZG-6020, SENXIN, China) to degas. Then 2 g of each mixture with different MRF content was taken and placed on the center of a dry and clean glass sheet (50 × 50 mm), spin-coated with a homogenizer (Spin-51, Shanghai Chemat Advanced Ceramics Technology Co., Ltd, China) at a speed of 500 rpm and time of 10 s, and then cured at 60 °C. The time required to fully cure the composite membrane was recorded as the curing time. For the samples with MRF content of 10, 15, 20, and 25 wt%, the curing time is 6, 12, 18, and 24 h, respectively.

Fabrication of the Liquid Gating Magnetoelastic Porous Membranes: The MPMs were fabricated by Laser Engraver (Spirit SI-25, GCC, USA) with the maximum power at 100 W, as shown in Figure S6 (Supporting Information). Firstly, template diagrams of the porous membranes were designed and drawn using CorelDRAW, including the shape and size of the membrane, the number and spacing of pores, and pore size. Then, by adjusting the power of the laser and the cutting speed, the pore size of the MPMs could be precisely controlled. After that, the LGMPMs were formed by infiltrating the functional gating liquid (all purchased from Sinopharm Chemical Reagent Co., Ltd.) of silicone oil, liquid paraffin, or Krytox 103 into the MPMs. The surfaces of porous membranes were dropped ≈10 μL cm^{-2} gating liquid, and uniform coverage was achieved after a while.

Deflection Measurements: The deflection was measured by a laser optical sensor ILD 2300–2 (206) (from Micro-Epsilon). The photo and the scheme of the experimental setup are shown in Figure S4 (Supporting Information). The MM was previously fixed in two poly(methyl methacrylate) (PMMA) sheets with a central hole of 6 mm in diameter and was deflected in a direction perpendicular to its surface under the external magnetic field by three bar permanent magnets, and the sensor recorded the deflection value. The strength of the field could be changed by varying the distance between the magnet and the membrane. Each measurement of the sample was carried out three times.

Supporting Information

Supporting Information is available from the Wiley Online Library or from the author.

Acknowledgements

J.L., X.X., and Y.L. contributed equally to this work. This work was supported by the National Key R&D Program of China (Project No. 2018YFA0209500), the National Natural Science Foundation of China (52025132, 21975209, 21621091, and 21808191), the Fundamental Research Funds for the Central Universities of China (20720190037), the 111 Project (B16029), and the National Science Foundation of Jiangsu Province (BK2021109).

Conflict of Interest

The authors declare no conflict of interest.

Data Availability Statement

The data that support the findings of this study are available from the corresponding author upon reasonable request.

Keywords

gas/liquid release, liquid gating technology, magnetoelastic membranes, meniscus-shaped deformations, mixture content monitoring

Received: September 15, 2021
Revised: October 18, 2021
Published online:

[1] a) X. Hou, *Adv. Mater.* **2016**, *28*, 7049; b) F. Gomollón-Bel, *Chem. Int.* **2020**, *42*, 3; c) J. Zhang, B. Chen, X. Chen, X. Hou, *Adv. Mater.* **2021**, 2005664; d) S. Yu, L. Pan, Y. Zhang, X. Chen, X. Hou, *Pure Appl. Chem.* **2021**, https://doi.org/10.1515/pac-2021-0402.

[2] a) H. Bazyar, S. Javadpour, R. G. H. Lammertink, *Adv. Mater. Interfaces* **2016**, *3*, 1600025; b) H. Bazyar, P. Lv, J. A. Wood, S. Porada, D. Lohse, R. G. H. Lammertink, *Soft Matter* **2018**, *14*, 1780; c) S. Wang, Y. Zhang, Y. Han, Y. Hou, Y. Fan, X. Hou, *Acc. Mater. Res.* **2021**, *2*, 407.

[3] a) X. Hou, Y. Hu, A. Grinthal, M. Khan, J. Aizenberg, *Nature* **2015**, *519*, 70; b) Z. Sheng, H. Wang, Y. Tang, M. Wang, L. Huang, L. Min, H. Meng, S. Chen, L. Jiang, X. Hou, *Sci. Adv.* **2018**, *4*, eaao6724; c) H. Bazyar, N. van de Beek, R. G. H. Lammertink, *Langmuir* **2019**, *35*, 9513.

[4] a) Z. Sheng, M. Zhang, J. Liu, P. Malgaretti, J. Li, S. Wang, W. Lv, R. Zhang, Y. Fan, Y. Zhang, *Natl. Sci. Rev.* **2021**, *8*, nwaa301; b) C. Wang, S. Wang, H. Pan, L. Min, H. Zheng, H. Zhu, G. Liu, W. Yang, X. Chen, X. Hou, *Sci. Adv.* **2020**, *6*, eabb4700.

[5] Y. Fan, Z. Sheng, J. Chen, H. Pan, B. Chen, F. Wu, S. Wang, X. Chen, X. Hou, *Angew. Chem., Int. Ed.* **2019**, *58*, 3967.

[6] B. Chen, R. Zhang, Y. Hou, J. Zhang, S. Chen, Y. Han, X. Chen, X. Hou, *Light: Sci. Appl.* **2021**, *10*, 127.

[7] a) Z. Liu, W. Wang, R. Xie, X. Ju, L. Chu, *Chem. Soc. Rev.* **2016**, *45*, 460; b) A. Zhang, K. Jung, A. Li, J. Liu, C. Boyer, *Prog. Polym. Sci.* **2019**, *99*, 101164; c) S. Bandehali, F. Parvizian, S. M. Hosseini, T. Matsuura, E. Drioli, J. Shen, A. Moghadassi, A. S. Adeleye, *Chemosphere* **2021**, *283*, 131207.

[8] a) J. Liu, L. Yu, G. Yue, N. Wang, Z. Cui, L. Hou, J. Li, Q. Li, A. Karton, Q. Cheng, L. Jiang, Y. Zhao, *Adv. Funct. Mater.* **2019**, *29*, 1808501; b) X. Fan, R. Xie, Q. Zhao, X. Li, X. Ju, W. Wang, Z. Liu, L. Chu, *J. Membr. Sci.* **2018**, *555*, 20; c) Q. Tan, H. Huang, Y. Peng, Y. Chang, Z. Zhang, D. Liu, C. Zhong, *J. Mater. Chem. A* **2019**, *7*, 26574; d) K. Xiao, Y. Zhou, X. Kong, G. Xie, P. Li, Z. Zhang, L. Wen, L. Jiang, *ACS Nano* **2016**, *10*, 9703.

[9] Z. Sheng, J. Zhang, J. Liu, Y. Zhang, X. Chen, X. Hou, *Chem. Soc. Rev.* **2020**, *49*, 7907.

[10] W. Lv, Z. Sheng, Y. Zhu, J. Liu, Y. Lei, R. Zhang, X. Chen, X. Hou, *Microsyst. Nanoeng.* **2020**, *6*, 43.

[11] Y. Han, Y. Zhang, M. Zhang, B. Chen, X. Chen, X. Hou, *Fundam. Res.*, https://doi.org/10.1016/j.fmre.2021.07.012.

[12] a) W. Hu, G. Z. Lum, M. Mastrangeli, M. Sitti, *Nature* **2018**, *554*, 81; b) J. Zhang, Y. Guo, W. Hu, M. Sitti, *Adv. Mater.* **2021**, *33*, 2100336; c) J. Zhang, Y. Guo, W. Hu, R. H. Soon, Z. S. Davidson, M. Sitti, *Adv. Mater.* **2021**, *33*, 2006191; d) P. Testa, R. W. Style, J. Cui, C. Donnelly, E. Borisova, P. M. Derlet, E. R. Dufresne, L. J. Heyderman, *Adv. Mater.* **2019**, *31*, 1900561; e) C. A. Brisbois, M. Tasinkevych, P. Vazquez-Montejo, M. Olvera de la Cruz, *Proc. Natl. Acad. Sci USA* **2019**, *116*, 2500; f) K. J. Merazzo, A. C. Lima, M. Rincón-Iglesias, L. C. Fernandes, N. Pereira, S. Lanceros-Mendez, P. Martins, *Mater. Horiz.* **2021**, *8*, 2654; g) V. Q. Nguyen, A. S. Ahmed, R. V. Ramanujan, *Adv. Mater.* **2012**, *24*, 4041.

[13] a) S. G. Sherman, A. C. Becnel, N. M. Wereley, *J. Magn. Magn. Mater.* **2015**, *380*, 98; b) W. Wang, J. V. I. Timonen, A. Carlson, D. M. Drotlef, C. T. Zhang, S. Kolle, A. Grinthal, T. Wong, B. Hatton, S. H. Kang, S. Kennedy, J. Chi, R. T. Blough, M. Sitti, L. Mahadevan, J. Aizenberg, *Nature* **2018**, *559*, 77; c) X. Zhang, L. Sun, Y. Yu, Y. Zhao, *Adv. Mater.* **2019**, *31*, 1903497; d) J. R. Morillas, J. de Vicente, *Soft Matter* **2020**, *16*, 9614.

[14] a) E. J. I. Barron, R. S. Peterson, N. Lazarus, M. D. Bartlett, *ACS Appl. Mater. Interfaces* **2020**, *12*, 50909; b) H. Huang, M. S. Sakar, A. J. Petruska, S. Pane, B. J. Nelson, *Nat. Commun.* **2016**, *7*, 12263; c) W. Lei, G. Hou, M. Liu, Q. Rong, Y. Xu, *Sci. Adv.* **2018**, *4*, eaau8767.

[15] N. Bira, P. Dhagat, J. R. Davidson, *Front. Rob. AI* **2020**, *7*, 146.

[16] a) A. K. Bastola, L. Li, M. Paudel, *J. Mater. Sci.* **2018**, *53*, 7004; b) Q. Ze, X. Kuang, S. Wu, J. Wong, S. M. Montgomery, R. Zhang, J. M. Kovitz, F. Yang, H. J. Qi, R. Zhao, *Adv. Mater.* **2020**, *32*, 1906657.

[17] W. Gao, L. Wang, X. Wang, H. Liu, *ACS Appl. Mater. Interfaces* **2016**, *8*, 14182.

[18] T. S. Wong, S. H. Kang, S. K. Tang, E. J. Smythe, B. D. Hatton, A. Grinthal, J. Aizenberg, *Nature* **2011**, *477*, 443.

[19] a) Y. Zhang, J. Guo, G. Han, Y. Bai, Q. Ge, J. Ma, C. Lau, L. Shao, *Sci. Adv.* **2021**, *7*, eabe8706; b) L. Liu, X. Huang, X. Zhang, K. Li, Y. Ji, C. Yu, C. Gao, *RSC Adv.* **2018**, *8*, 15102.

[20] a) C. A. Hone, C. O. Kappe, *Chem. - Eur. J.* **2020**, *26*, 13108; b) J. Qian, C. Hou, X. Li, Z. Jin, *Micromachines* **2020**, *11*, 172.

[21] a) D. Drotman, S. Jadhav, D. Sharp, C. Chan, M. T. Tolley, *Sci. Rob.* **2021**, *6*, eaay2627; b) L. Belding, B. Baytekin, H. T. Baytekin, P. Rothemund, M. S. Verma, A. Nemiroski, D. Sameoto, B. A. Grzybowski, G. M. Whitesides, *Adv. Mater.* **2018**, *30*, 1704446.

[22] a) Q. He, D. O. Kiesewetter, Y. Qu, X. Fu, J. Fan, P. Huang, Y. Liu, G. Zhu, Y. Liu, Z. Qian, X. Chen, *Adv. Mater.* **2015**, *27*, 6741; b) Z. Jin, Y. Wen, L. Xiong, T. Yang, P. Zhao, L. Tan, T. Wang, Z. Qian, B. Su, Q. He, *Chem. Commun.* **2017**, *53*, 5557; c) E. Palao, T. Slanina, L. Muchova, T. Solomek, L. Vitek, P. Klan, *J. Am. Chem. Soc.* **2016**, *138*, 126; d) W. Fan, B. C. Yung, X. Chen, *Angew. Chem., Int. Ed.* **2018**, *57*, 8383.

[23] a) D. Jovanov, B. Vujic, G. Vujic, *J. Environ. Manage.* **2018**, *216*, 32; b) Q. Lyu, J. Tan, L. Li, Y. Ju, A. Busch, D. A. Wood, P. G. Ranjith, R. Middleton, B. Shu, C. Hu, Z. Wang, R. Hu, *Energy Environ. Sci.* **2021**, *14*, 4203.